ISBN: 978-3-95450-219-6 ISSN: 2226-0366 doi: 10.18429/JACoW-LINAC2024-THAA010

DUST CONTAMINATION IN THE TRIUMF E-LINAC

A. Mahon*[1], T. Junginger[1], J. Keir, P. Kolb, D. Lang, T. Planche[1] TRIUMF, Vancouver, Canada
[1]also at University of Victoria, Victoria, Canada

Abstract

The presence of dust particulates inside the vacuum space of particle accelerators has been linked to a variety of issues: At the Large Hadron Collider (LHC), beam loss events have been linked to the interaction of charged dust with the proton beams. In superconducting rf cavities, dust contamination leads to field emission, limiting the accelerating gradient and causing damage to external beamline components. Facilities such as the TRIUMF electron linear accelerator see progressive onsets in field emission that cannot simply be explained by vacuum events. The environment of a particle accelerator provides an ideal opportunity for dust to gain charge, which is one of the main drivers of dust grain dynamics in vacuum. However, fundamental parameters such as the dust composition and charge to mass ratio of these grains are unique to each accelerator environment and remain largely unknown. We will present an analysis of dust samples taken from TRIUMF linear accelerators, detailing their size, composition and potential sources.

INTRODUCTION

TRIUMF is undertaking a significant expansion of its rare isotope program via the addition of the Advanced Rare IsotopE Laboratory (ARIEL). The ARIEL facility will add two new target stations to increase isotope production; one will be driven by a 520 MeV proton beam from the existing cyclotron, the other by a 30 MeV electron beam from a recently commissioned superconducting electron linear accelerator, the e-Linac (Fig. 1). The electron beam will be used to generate high purity isotope products via photofission, a technique which yields more isotopes in the neutron rich region of the nuclear landscape [1].

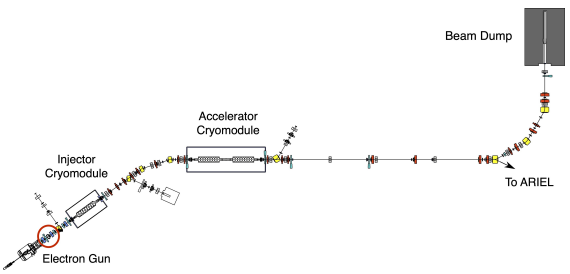

Figure 1: Schematic of ARIEL e-Linac.

High Gradient Requirements

As the overall isotope production yield at ARIEL is expected to depend strongly on the electron beam energy [2], maintaining the output at – or above – 30 MeV is essential for the ARIEL science program. Three 1.3 GHz 9-cell elliptical superconducting rf (SRF) cavities, made of bulk niobium, are used to accelerate the electron beam. To reach the design specification of 30 MeV, each cavity must deliver an energy gain of 10 MeV or higher. Figure 2 demonstrates the steep dropoff in isotope production when the electron beam energy, and by association the SRF accelerating gradient, dips below this operational imperative.

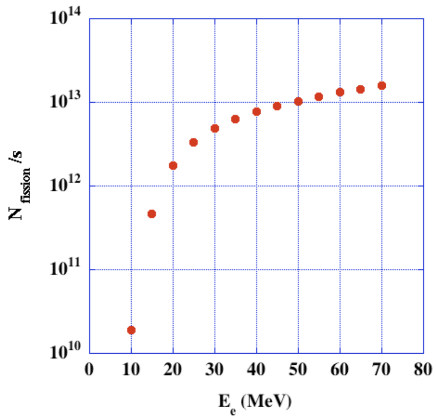

Figure 2: Isotope photofission yield as a function of 100kW electron beam energy [2].

Present Limitations

One practical limitation in SRF cavities is field emission [3], wherein rogue electrons are emitted from regions of high surface electric field inside the cavities. Field emission electrons cause a range of detrimental effects in accelerators. They draw energy from the rf field, lowering the quality factor (Q) of the resonator [4]. This increases the heat being dissipated in the cavity surface, requiring more liquid helium consumption to maintain cryogenic temperatures at the same gradient, ultimately forcing facilities with finite cryo power to operate at lower gradients. Field emission electrons may also reach relativistic velocities and generate intense bremsstrahlung and radiation damage to accelerator components [5–7].

The TRIUMF e-Linac actively suffers from field emission, which can be observed directly with our viewscreen diagnostics elements. Field emission electrons are accelerated by the rf fields present in the cavities, and can consequently travel outside of the confines of the cavity, which can then be picked up on our scintillator screens. An example of this is shown in Fig. 3; in this case the field emission electrons are escaping the confines of the adjacent cavity to reach the viewscreen further down the beamline. We are able to identify these particles as electrons, and not for example X-rays, as we are able to steer them with the optical elements of the beamline, proving that they are charged particles.

* amahon@triumf.ca

ISBN: 978-3-95450-219-6 ISSN: 2226-0366 doi: 10.18429/JACoW-LINAC2024-THAA010

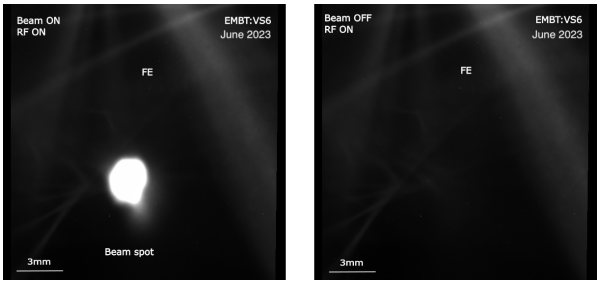

Figure 3: Left: Viewscreen image from the medium energy section of the e-Linac with both beam and rf turned on. Beam is visible as a large bright spot in the centre. Image is overexposed to highlight the field emission electrons appearing like spotlights at the top of the image. Right: Same viewscreen image from the medium energy section of the e-Linac with rf on but beam off. Note the field emission electrons at the top of the image remain, indicating they are coming from the adjacent cryomodule and not the beam.

Research conducted at SRF facilities confirmed micron-sized particulates on the inner surface to be the main triggers of field emission in their cavities [8, 9]. Great care is taken to install SRF cavities, however the field emission onset deteriorates over time, and foreign particulates are routinely found inside cavities post operation. The mechanism that moves these dust particulates from less clean sections of beamline into the ultra-clean niobium cavities during operation, even in the absence of vacuum incidents, remains unclear. The environment of a particle accelerator provides an ideal opportunity for dust to gain charge, which is believed to be one of the main drivers of dust dynamics in vacuum [10]. Understanding this effect would open a path towards long-term reliable operations of superconducting rf accelerators at their maximum accelerating gradient and with maximum power efficiency. This prompted a more detailed study of the presence of particulates in the TRIUMF e-Linac to better understand the accelerator environment.

PARTICULATE COLLECTION AND CHARACTERIZATION

To have an accurate representation of the e-Linac environment, it is imperative to understand the types of particulates that currently contaminate the system. Samples were collected from the electron gun section of the accelerator in August 2023, when this section was vented and opened for maintenance. This collection was restricted to a section of beampipe due primarily to access issues, however we also did not want to risk introducing contaminants to the cavities by sampling their surface directly.

Procedure

Particulates were collected directly from the inner surface of a diagnostics box through a blank flange, using double sided carbon tape mounted onto pin stubs (Fig. 4). Each sample was pressed down firmly on the bottom, top, left and right inner surface of the diagnostics box opening, as well as from the inner surface of the flange itself. Tweezers were used to remove the cover on the tabs, and a clamp was used to transfer them in and out of the storage box. Each sample was pressed down only once in one specific area for approximately 3 seconds. Control samples were also taken, wherein the same handling and storing procedures were executed, with the exception of the actual particulate collection, to quantify any contamination that may be externally introduced during the handling process.

Figure 4: Picture of sample storage box: Samples on the left side of the box were collected from the gun section of the e-Linac and have been coated in carbon for SEM analysis. Samples on the right show pre-mounted stubs with covers still in place as they were not used for collection.

These samples were then analyzed via scanning electron microscopy (SEM), using energy dispersive X-ray spectroscopy (EDX) to identify their composition. This was done at the UBC department of Materials Engineering lab, where they underwent carbon coating prior to analysis, such as to prevent charging of any potentially non conductive pieces of dust collected when exposed to the electron beam of the microscope.

The SEM used to analyse these samples is a FEI Quanta 650, which uses a tungsten filament to produce the electron beam. This machine can detect both BSE and SE, which yield two complimentary images of a given sample. This microscope is also equipped with a large area EDX detector, with Esprit 2.1.2 Software from Bruker that allows for automated particle analysis. An electron beam energy of 20 keV was used during this analysis, with an EDX pulse rate of 400 kcps (kilo counts per second).

Results and Analysis

Figure 5 shows a closer look at how these contaminating particulates appear under the microscope. The EDX spectrum from both grains show in Fig. 5 are presented in Fig. 6. These figures show the peaks in the X-ray energy spectrum, which are matched with the characteristic X-ray energies of specific elements to identify them.

A total of 87 e-Linac dust grains and 5 control grains were analysed. A summary of their elemental composition is presented in Fig. 7. These results are normalized with respect to the number of grains analysed, in addition to

ISBN: 978-3-95450-219-6 ISSN: 2226-0366 doi: 10.18429/JACoW-LINAC2024-THAA010

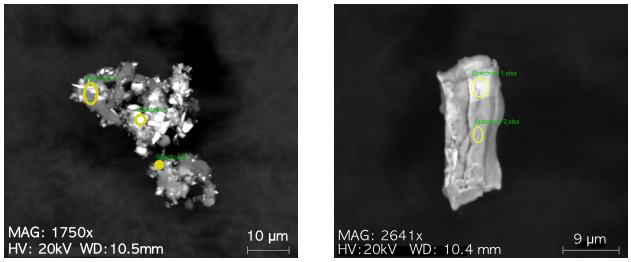

Figure 5: SEM images of e-Linac dust grains. Yellow circles indicate the areas used in the EDX analysis.

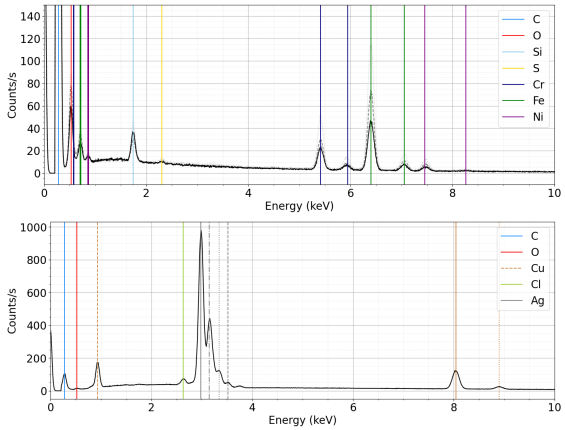

Figure 6: Spectrum of X-ray energies obtained from EDX analysis of dust grains shown in Fig. 5. Characteristic x-ray energies obtained from LBNL x-ray data booklet [11] are matched to the peaks seen in the spectra to identify elements.

the density of the grains on the sample, to more accurately compare between the control and beamline samples. The density of the grains on the sample was determined with the help of an image processing code, which identified the bright spots on the image as dust grains (Fig. 8).

Table 1 presents possible sources of the elements found in the EDX analysis. As expected some of these elements come from external contamination e.g. potassium, however many of them find their origin from components inside the beamline, indicating that these dust grains may be generated in-situ. In particular, some of the elements identified can be traced to a target test stand, which was located at the end of beamline perpendicular to the low energy section of the e-Linac (Fig. 1). This test stand explored various materials for the electron-gamma converter for the ARIEL electron target, including gold and aluminium [12]. Note this list is non exhaustive.

CONCLUSION

With this clearer understanding of dust composition and origin, the main questions that remain to be answered are: what sign and magnitude of charge is acquired by the dust in TRIUMF's accelerator environment; how do they detach from the surface of the vacuum chamber; and what drives their migration along the beamline. Answering these questions is necessary to devise an effective method for mitigating field emission in superconducting linacs. An offline test setup has been conceived and is under assembly in order to test the leading hypothesis, and results are expected within the coming year.

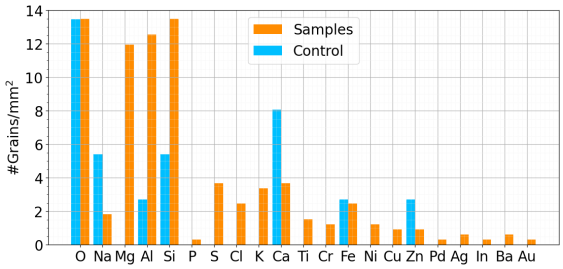

Figure 7: Composition of dust collected from the e-Linac. Elements found in beamline samples are in orange, while elements found in control samples are in blue.

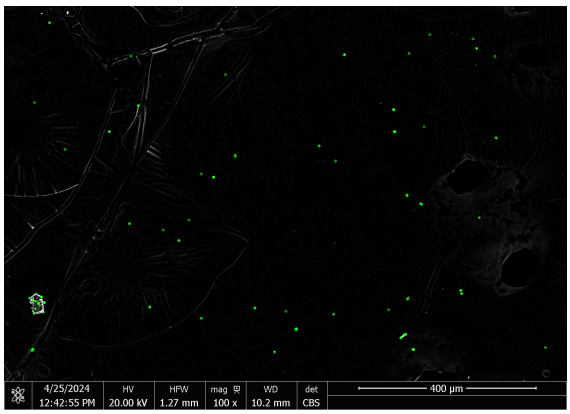

Figure 8: Zoomed out image of dust sample to visualize the density of grains on a larger surface. Edge detection based image processing code was used to identify and count dust grains to determine their density over a given area.

Table 1: Potential Sources for Elements Identified via EDX

Element	Source
Al/Pd/Au	Test stand/electrical connectors
Si	Ceramics, concrete
K	Human contamination
Stainless Steel (Fe/Ni/Cr)	Most beamline elements
Cu/Ag	Braising, anode electrodes
Ti	Cathode electrodes
In/Ba	Cathode material

ACKNOWLEDGEMENTS

I would like acknowledge the support of the Natural Sciences and Engineering Research Council of Canada (NSERC). This work was conducted on the traditional, ancestral, and unceded territory of the *xʷməθkʷəy̓əm* (Musqueam) people.

ISBN: 978-3-95450-219-6 ISSN: 2226-0366 doi: 10.18429/JACoW-LINAC2024-THAA010

REFERENCES

[1] W. T. Diamond, "A radioactive ion beam facility using photofission", *Nucl. Instrum. Methods Phys. Res., Sect. A*, vol. 432, no. 2-3, pp. 471–482, 1999.

[2] G. Hackman, "ARIEL: TRIUMF's advanced rare isotope laboratory", *Act. Phys. Pol. B*, vol. 45, p. 503, 2014. doi:10.5506/APhysPolB.45.503

[3] A. Arnold *et al.*, "More than 15 Years of CW SRF Operation at ELBE", Dresden, Germany, Aug. 2019.

[4] J. Knoblock, "Field emission and thermal breakdown in superconducting niobium cavities for accelerators", *IEEE Trans. Appl. Supercond.*, vol. 9, no. 2, pp. 1016–1022, 1999. doi:10.1109/77.783471

[5] C. Reece, "Operating experience with superconducting cavities at Jefferson lab", *Part. Accel.*, vol. 60, pp. 43–52, 1998.

[6] S.-p. Yoon, H.-s. Kim, H.-j. Kwon, and Y.-s. Cho, "Radiation shielding design to attenuate bremsstrahlung x-rays induced by field emission electrons at the vertical SRF cavity test", in *Trans. Korean Nucl. Soc. Autumn Meet.,* Gyeongju, Korea, Oct. 2011, 2011.

[7] R. L. Geng, J. F. Fischer, E. A. McEwen, and O. Trofimova, "Nature and Implication of Found Actual Particulates on the Inner Surface of Cavities in a Full-Scale Cryomodule Previously Operated With Beams", in *Proc. SRF'15*, Whistler, Canada, Sep. 2015, pp. 164–168. https://jacow.org/SRF2015/papers/MOPB035.pdf.

[8] U. Klein and J. Turneaure, "Field emission in superconducting rf cavities", *IEEE Trans. Magn.*, vol. 19, no. 3, pp. 1330–1333, 1983. doi:10.1109/TMAG.1983.1062420

[9] C. Z. Antoine *et al.*, "Dust Contamination During Chemical Treatment of RF Cavities: Symptoms and Cures", in *Proc. SRF'91*, Hamburg, Germany, Aug. 1991. https://jacow.org/SRF91/papers/SRF91E09.pdf.

[10] P. Bélanger *et al.*, "Charging mechanisms and orbital dynamics of charged dust grains in the lhc", *Phys. Rev. Accel. Beams*, vol. 25, no. 10, p. 101 001, 2022. doi:10.1103/PhysRevAccelBeams.25.101001

[11] C. for X-ray Optics and L. B. N. L. Advanced Light Source, *X-ray data booklet*, LBNL/PUB-490, Rev. 3, 2009. https://xdb.lbl.gov/

[12] L. Egoriti, M. Cervantes, T. Day Goodacre, and A. Gottberg, "Material development towards a solid 100 kw electron-gamma converter for triumf-ariel", *Nucl. Instrum. Methods Phys. Res., Sect. B*, vol. 463, pp. 232–236, 2020. doi:https://doi.org/10.1016/j.nimb.2019.05.031